Dyadic Green's function of an ideal hard surface circular waveguide with application to excitation and scattering problems

Victor A. Klymko, Alexander B. Yakovlev, Islam A. Eshrah,
Ahmed A. Kishk, and Allen W. Glisson

Center for Applied Electromagnetic Systems Research, Department of Electrical Engineering, University of Mississippi, University, Mississippi, USA

Received 1 September 2004; revised 28 February 2005; accepted 11 March 2005; published 22 June 2005.

[1] Green's function analysis of ideal hard surface circular waveguides is proposed with application to excitation and scattering problems. A decomposition of the hard surface waveguide into perfect electric conductor and perfect magnetic conductor waveguides allows the representation of dyadic Green's function in terms of transverse electric (TE) and transverse magnetic (TM) waveguide modes, respectively. In addition, a term corresponding to a transverse electromagnetic (TEM) mode is included in the representation of the Green's dyadic. The TEM term is extracted in closed form from the eigenmode expansion of TM and TE modes in the zero-cutoff limit. The electric field distribution due to an arbitrarily oriented electric dipole source is illustrated for representative TM, TE, and TEM modes propagating in the ideal hard surface circular waveguide. The derived Green's function is used in the method of moments analysis of an ideal hard surface waveguide excited by a half-wavelength strip dipole antenna. In addition, the scattering of the TEM mode by a thin strip is studied in the ideal hard surface circular waveguide.

Citation: Klymko, V. A., A. B. Yakovlev, I. A. Eshrah, A. A. Kishk, and A. W. Glisson (2005), Dyadic Green's function of an ideal hard surface circular waveguide with application to excitation and scattering problems, *Radio Sci.*, *40*, RS3014, doi:10.1029/2004RS003167.

1. Introduction

[2] Artificial surfaces with anisotropic impedance, characterized as hard and soft surfaces, have been introduced in electromagnetics in the past two decades. A planar hard surface is realized by loading a conducting surface with dielectric-filled corrugations in the direction of wave propagation, whereas a soft surface is implemented by using transverse corrugations with respect to the propagating direction [*Kildal*, 1988a, 1990]. A planar hard surface can also be realized by using longitudinal periodic metal strips placed on the dielectric coating of a metal surface [*Aas*, 1991]. A hard surface cylindrical waveguide is implemented by introducing longitudinal dielectric-filled corrugations [*Kildal*, 1990] or by lining the perfect electric conductor (PEC) waveguide with a dielectric coating loaded with narrow longitudinal PEC strips [*Kishk and Morgan*, 2001].

0048-6604/05/2004RS003167$11.00

[3] Different approaches have been used for the analysis of scattering from soft and hard surfaces. *Lindell* [1995] applied the image theory for a planar anisotropic surface by decomposing the original source above the surface in two components to generate the transverse electric (TE) and transverse magnetic (TM) polarized fields with respect to the direction of corrugations. An open hard surface is studied by *Sipus et al.* [1996] by considering a grounded dielectric slab illuminated by a spectrum of plane waves with no component of the electric field in the direction of propagation along the surface. The three-dimensional scattering from the infinite and semi-infinite plain surfaces with anisotropic impedance is analyzed by *Nepa et al.* [2001], and scattering from the edges of anisotropic impedance surfaces is studied by *Manara et al.* [2000]. The asymptotic boundary conditions (ASBC) are applied by *Kishk et al.* [1998] instead of using the Floquet mode expansions for the problem of scattering from a cylinder with dielectric-filled corrugations. The scattering from dielectric cylinders loaded with longitudinal or circumferential

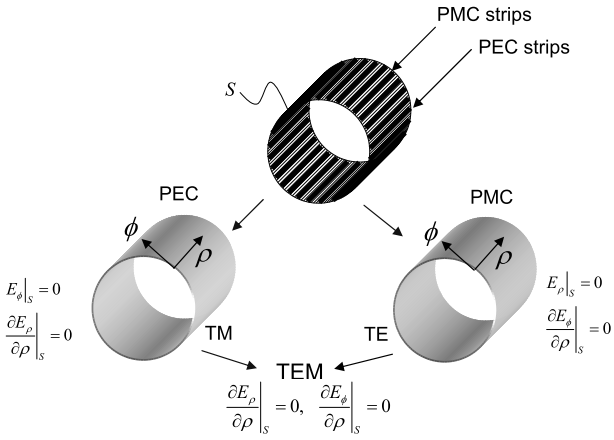

Figure 1. PEC/PMC strip model for an ideal hard surface circular waveguide. The hard surface behaves like a PEC waveguide for TM modes and as a PMC waveguide for TE modes. A TEM mode is obtained as a contribution of TM and TE modes in the zero-cutoff limit. The TEM mode "sees" the ideal hard surface waveguide as a combination of PEC and PMC waveguides, and it satisfies the boundary conditions on the ideal hard surface partially contributed by PEC and PMC waveguides, that is, $\partial E_\rho/\partial\rho|_S = 0$, $\partial E_\phi/\partial\rho|_S = 0$. See color version of this figure at back of this issue.

metal strips illuminated at oblique incidence is studied by *Kishk and Kildal* [1997] by using the ASBC approach. Also, the ASBC has been used by *Kishk* [2003] in the analysis of cylindrical hard surfaces of arbitrarily shaped cross section.

[4] Artificial hard surfaces are primarily utilized in hard horn antennas in order to create a transverse electromagnetic (TEM) wave propagation regime with a uniform field distribution over the horn aperture and zero cross-polarization [*Kildal*, 1988b]. The use of a hard horn antenna increases directivity and decreases beam width for given aperture dimensions [*Lier and Kildal*, 1988]. Also, an infinite planar array of open-ended rectangular waveguides with dielectric-loaded walls results in a better matching of the array to free space and increase of the aperture and gain to remove the scan blindness [*Skobolev and Kildal*, 1998]. The performance of an open-ended circular waveguide with strip-loaded dielectric hard walls used as the element of antenna arrays is also studied by *Skobolev and Kildal* [2000].

[5] Recent developments in the application of hard surfaces are reported by *Yang et al.* [1999], wherein a photonic band gap (PBG) structure implemented on sidewalls of rectangular waveguide has been used to create the TEM mode propagation. Also, a rectangular waveguide with sidewalls covered by the printed dipole frequency selective surface (FSS) has been designed to obtain the quasi-TEM mode [*Cucini et al.*, 2004; *Maci et al.*, 2005].

[6] In this work, Green's function analysis of an ideal hard surface circular waveguide is proposed in order to create a TEM wave propagation with application to excitation and scattering problems. The modal characterization of an ideal hard surface waveguide gives a physical insight into the behavior of modes supported by practical hard surface waveguides. The developed Green's function provides a powerful framework for the efficient analysis of the ideal hard surface circular waveguide, which serves as an initial step in the analysis and design of waveguides with physical hard surface. In the proposed approach, the ideal structure is decomposed into PEC and perfect magnetic conductor (PMC) waveguides, which independently support TM and TE modes, respectively. In addition, it is shown that the TEM mode with a uniform field propagates in the ideal hard surface circular waveguide. On the basis of the modal analysis of the structure, the electric dyadic Green's function due to an arbitrarily oriented electric dipole source is obtained in the eigenmode expansion form in terms of TM modes of the PEC waveguide, TE modes of the PMC waveguide, and the TEM mode. The TEM term of the Green's dyadic is extracted from the eigenmode expansion in the zero-cutoff limit. The electric field distribution due to an arbitrarily oriented electric dipole source is illustrated for representative TM, TE, and TEM modes propagating in the ideal hard surface circular waveguide. The Green's function derived is used in the method of moments analysis of ideal hard surface waveguide excitation by a half-wavelength strip dipole antenna. In addition, the scattering of the TEM mode by a thin strip is studied in the ideal hard surface circular waveguide.

2. Dyadic Green's Function of an Ideal Hard Surface Circular Waveguide

[7] The ideal hard surface circular waveguide is modeled by alternating PEC and PMC longitudinal strips (in the propagating direction) with vanishing widths [*Ruvio et al.*, 2003]. The PEC and PMC strips enforce the annulment of the longitudinal electric and magnetic fields, respectively. This results in decomposition of the original hard surface waveguide into PEC and PMC waveguides, which individually support TM and TE waveguide modes, respectively. In addition, a hard surface waveguide as a multiconductor transmission line also supports a TEM mode. This mode is obtained as a contribution of TM and TE modes of PEC and PMC waveguides in the zero-cutoff limit.

[8] The concept of the ideal hard surface circular waveguide as a composition of PEC and PMC waveguides is illustrated in Figure 1.

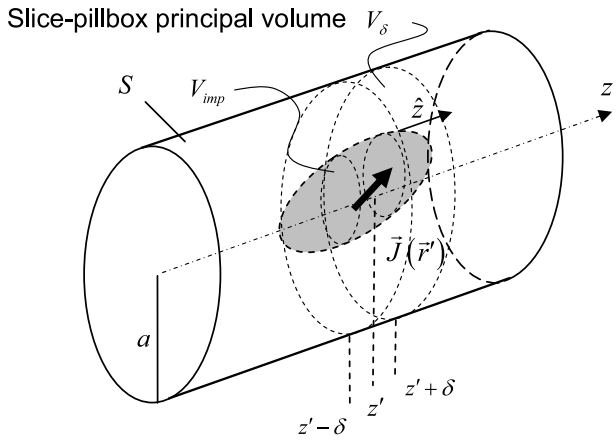

Figure 2. Geometry of an ideal hard surface circular waveguide with the impressed electric current source. A slice-pillbox principal volume associated with the source-plane singularity of the Green's function at $z = z'$ is shown in the source region.

[9] In Figure 1, ρ is the normal direction to the waveguide boundary and ϕ is the tangential direction to the waveguide boundary and transverse to the longitudinal strips. When the hard surface behaves like a PEC conductor, E_ϕ and the normal derivative of E_ρ are zero on the waveguide surface S, that is, $E_\phi|_S = 0$ and $\partial E_\rho/\partial\rho|_S = 0$, and when the hard surface behaves like a PMC conductor, E_ρ and the normal derivative of E_ϕ are zero on the waveguide surface S, that is, $E_\rho|_S = 0$ and $\partial E_\phi/\partial\rho|_S = 0$, and vice versa for the magnetic field components.

[10] Consider an ideal hard surface circular waveguide with the impressed electric current source shown in Figure 2. The electric field in the waveguide (including the source region) is expressed in the integral form,

$$\mathbf{E}(\mathbf{r}) = -j\omega\mu_0 \int_{V_{imp}} \overline{\mathbf{G}}(\mathbf{r},\ \mathbf{r}') \cdot\ \mathbf{J}(\mathbf{r}')dV', \qquad (1)$$

where $\overline{\mathbf{G}}(\mathbf{r}, \mathbf{r}')$ is the electric dyadic Green's function of the ideal hard surface circular waveguide obtained as the solution of a dyadic wave equation,

$$\nabla \times \nabla \times \overline{\mathbf{G}}(\mathbf{r},\ \mathbf{r}') - k_0^2 \overline{\mathbf{G}}(\mathbf{r},\ \mathbf{r}') = \overline{\mathbf{I}}\delta(\mathbf{r} - \mathbf{r}'), \qquad (2)$$

where $k_0 = \omega\sqrt{\varepsilon_0\mu_0}$.

[11] The dyadic Green's function is obtained in the eigenmode expansion form as a superposition of three parts associated with the TM modes of the PEC waveguide, TE modes of the PMC waveguide, and the TEM mode of the ideal hard surface,

$$\overline{\mathbf{G}}(\mathbf{r},\ \mathbf{r}') = \overline{\mathbf{G}}^{TM}(\mathbf{r},\ \mathbf{r}') + \overline{\mathbf{G}}^{TE}(\mathbf{r},\ \mathbf{r}') + \overline{\mathbf{G}}^{TEM}(\mathbf{r},\ \mathbf{r}'). \quad (3)$$

[12] This corresponds to decomposition of the boundary value problem for the Green's function into three problems. Thus $\overline{\mathbf{G}}^{TM}(\mathbf{r}, \mathbf{r}')$ part of the Green's function satisfies the first-kind boundary conditions on S (equivalent to those for the tangential electric field on PEC),

$$\hat{\boldsymbol{\rho}} \times \overline{\mathbf{G}}^{TM}(\mathbf{r},\ \mathbf{r}')\Big|_S = \overline{\mathbf{0}}, \qquad (4)$$

where $\hat{\boldsymbol{\rho}}$ is the normal in the radial direction (in cylindrical coordinates) to S; $\overline{\mathbf{G}}^{TE}(\mathbf{r}, \mathbf{r}')$ part satisfies the second-kind boundary conditions on S (equivalent to the behavior of electric field on PMC),

$$\begin{aligned} \hat{\boldsymbol{\rho}} \times \nabla \times \overline{\mathbf{G}}^{TE}(\mathbf{r},\ \mathbf{r}')|_S &= \overline{\mathbf{0}} \\ \hat{\boldsymbol{\rho}} \cdot \overline{\mathbf{G}}^{TE}(\mathbf{r},\ \mathbf{r}')\Big|_S &= \mathbf{0}. \end{aligned} \qquad (5)$$

[13] The TEM part of the Green's function satisfies mixed boundary conditions, which are equivalent to those for normal and tangential components of the electric field, $\partial E_\rho/\partial\rho|_S = 0$ and $\partial E_\phi/\partial\rho|_S = 0$, (shown in Figure 1),

$$\begin{aligned} \hat{\boldsymbol{\rho}} \cdot \nabla\left(\hat{\boldsymbol{\rho}} \cdot \overline{\mathbf{G}}^{TEM}(\mathbf{r},\ \mathbf{r}')\right)\Big|_S &= \mathbf{0} \\ \hat{\boldsymbol{\rho}} \cdot \nabla\left(\hat{\boldsymbol{\phi}} \cdot \overline{\mathbf{G}}^{TEM}(\mathbf{r},\ \mathbf{r}')\right)\Big|_S &= \mathbf{0}. \end{aligned} \qquad (6)$$

[14] The electric Green's dyadic of the ideal hard surface waveguide is expressed in terms of solenoidal and irrotational parts [*Collin*, 1991; *Johnson et al.*, 1979],

$$\begin{aligned} \overline{\mathbf{G}}(\mathbf{r},\ \mathbf{r}') = \frac{1}{2j\omega\mu_0} PV\Big\{ & \mathbf{E}^{TEM}(\mathbf{r})\mathbf{E}^{TEM}(\mathbf{r}') \\ & + \sum_{s=0}^{\infty}\sum_{k=1}^{\infty}\left(\mathbf{E}_{sk}^{TM}(\mathbf{r})\mathbf{E}_{sk}^{TM}(\mathbf{r}') + \mathbf{E}_{sk}^{TE}(\mathbf{r})\mathbf{E}_{sk}^{TE}(\mathbf{r}')\right)\Big\} \\ & - \overline{\mathbf{L}}\frac{\delta(\mathbf{r} - \mathbf{r}')}{k_0^2}. \end{aligned} \qquad (7)$$

[15] The solenoidal part is obtained in the form of eigenmode expansion of TM, TE, and TEM modes and understood in the principal value (PV) sense [*Yaghjian*, 1982; *Chew*, 1989; *Eshrah et al.*, 2004]. The irrotational part includes a depolarizing dyadic $\overline{\mathbf{L}}$ associated with a specific principal exclusion volume [*Yaghjian*, 1980]. A slice-pillbox principal volume with the normal in the propagating z direction (Figure 2) [*Eshrah et al.*, 2004; *Yaghjian*, 1980; *Wang*, 1982; *Viola and Nyquist*, 1988] is used in this formulation with $\overline{\mathbf{L}} = \hat{\mathbf{z}}\hat{\mathbf{z}}$. The main singularity of the Green's function is contained in the solenoidal part and represents a source-plane singularity at $z = z'$. It is understood as an improper integral with the slice-pillbox principal volume.

[16] The electric field inside the waveguide given by (1) is uniquely defined as the sum of the improper integral of the solenoidal part understood in the principal value sense and the integral of the irrotational part over the entire volume of the impressed current source,

$$\mathbf{E}(\mathbf{r}) = -\frac{1}{2}\lim_{\delta\to 0}\int_{V_{imp}-V_\delta}\Big(\mathbf{E}^{TEM}(\mathbf{r})\mathbf{E}^{TEM}(\mathbf{r}') + \sum_{s=0}^{\infty}\sum_{k=1}^{\infty}\big(\mathbf{E}_{sk}^{TM}(\mathbf{r})\mathbf{E}_{sk}^{TM}(\mathbf{r}') + \mathbf{E}_{sk}^{TE}(\mathbf{r})\mathbf{E}_{sk}^{TE}(\mathbf{r}')\big)\Big) \cdot \mathbf{J}(\mathbf{r}')dV' - \hat{\mathbf{z}}\frac{J_z(\mathbf{r})}{j\omega\varepsilon_0}. \quad (8)$$

[17] Below we derive the electric and magnetic fields of TM and TE eigenmodes of PEC and PMC waveguides, respectively. The electric fields of TM and TE eigenmodes propagating in the positive, "+", and negative, "−", z direction, $\mathbf{E}_{sk}^{TM\pm}(\mathbf{r})$ and $\mathbf{E}_{sk}^{TE\pm}(\mathbf{r})$, are expressed in terms of electric vector wave functions [*Collin*, 1991],

$$\mathbf{E}_{sk}^{TM\pm}(\mathbf{r}) = \big(\mathbf{e}_{sk}^{TM}(\rho,\phi) \pm \hat{\mathbf{z}}e_{z,sk}(\rho,\phi)\big)e^{\mp\gamma_{sk}z}$$
$$\mathbf{E}_{sk}^{TE\pm}(\mathbf{r}) = \mathbf{e}_{sk}^{TE}(\rho,\phi)e^{\mp\gamma_{sk}z}. \quad (9)$$

[18] The corresponding magnetic fields of TM and TE eigenmodes are obtained in terms of magnetic vector wave functions,

$$\mathbf{H}_{sk}^{TM\pm}(\mathbf{r}) = \pm\mathbf{h}_{sk}^{TM}(\rho,\phi)e^{\mp\gamma_{sk}z}$$
$$\mathbf{H}_{sk}^{TE\pm}(\mathbf{r}) = \big(\pm\mathbf{h}_{sk}^{TE}(\rho,\phi) + \hat{\mathbf{z}}h_{z,sk}(\rho,\phi)\big)e^{\mp\gamma_{sk}z}. \quad (10)$$

[19] The longitudinal components of electric and magnetic fields, $e_{z,sk}(\rho,\phi)$ and $h_{z,sk}(\rho,\phi)$, satisfy Helmholtz's equation in cylindrical coordinates,

$$\frac{\partial^2}{\partial\rho^2}e_{z,sk}(\rho,\phi) + \frac{1}{\rho}\frac{\partial}{\partial\rho}e_{z,sk}(\rho,\phi) + \frac{1}{\rho^2}\frac{\partial^2}{\partial\phi^2}e_{z,sk}(\rho,\phi) + k_{c,sk}^2 e_{z,sk}(\rho,\phi) = 0$$
$$\frac{\partial^2}{\partial\rho^2}h_{z,sk}(\rho,\phi) + \frac{1}{\rho}\frac{\partial}{\partial\rho}h_{z,sk}(\rho,\phi) + \frac{1}{\rho^2}\frac{\partial^2}{\partial\phi^2}h_{z,sk}(\rho,\phi) + k_{c,sk}^2 h_{z,sk}(\rho,\phi) = 0. \quad (11)$$

[20] The solution of (11) is obtained by separating the variables,

$$e_{z,sk}(\rho,\phi) = \alpha_{sk}^{TM}J_s\big(k_{c,sk}\rho\big)\cos(s\phi) + \beta_{sk}^{TM}J_s\big(k_{c,sk}\rho\big)\sin(s\phi)$$
$$h_{z,sk}(\rho,\phi) = \alpha_{sk}^{TE}J_s\big(k_{c,sk}\rho\big)\sin(s\phi) + \beta_{sk}^{TE}J_s\big(k_{c,sk}\rho\big)\cos(s\phi) \quad (12)$$

where J_s is the Bessel function of the first kind of order s and $k_{c,sk}$ are the cutoff wave numbers of TM and TE modes determined as roots of the characteristic equation,

$$J_s\big(k_{c,sk}a\big) = 0. \quad (13)$$

This implies that the ideal hard surface circular waveguide supports degenerate TM and TE modes with the same cutoff wave numbers and the same propagation constants, $\gamma_{sk} = \sqrt{k_{c,sk}^2 - k_0^2}$.

[21] The solution in (12) represents the superposition of two orthogonal polarizations (associated with the sine and cosine terms). Since one polarization can be obtained from the other by 90° rotation of coordinates, only one polarization will be considered in the derivations to follow. Thus the transverse electric vector wave functions are expressed in terms of $e_{z,sk}$ and $h_{z,sk}$,

$$\mathbf{e}_{sk}^{TM} = -\frac{\gamma_{sk}}{k_{c,sk}^2}\nabla_t e_{z,sk} = \frac{\gamma_{sk}}{k_{c,sk}}\Big\{-\hat{\boldsymbol{\rho}}\alpha_{sk}^{TM}J_s'\big(k_{c,sk}\rho\big)\cos(s\phi) + \hat{\boldsymbol{\phi}}\frac{s}{k_{c,sk}\rho}\alpha_{sk}^{TM}J_s\big(k_{c,sk}\rho\big)\sin(s\phi)\Big\} \quad (14)$$

$$\mathbf{e}_{sk}^{TE} = \frac{j\omega\mu_0}{k_{c,sk}^2}\hat{\mathbf{z}}\times\nabla_t h_{z,sk} = \frac{j\omega\mu_0}{k_{c,sk}}\Big\{-\hat{\boldsymbol{\rho}}\frac{s}{k_{c,sk}\rho}\alpha_{sk}^{TE}J_s\big(k_{c,sk}\rho\big)\cos(s\phi) + \hat{\boldsymbol{\phi}}\alpha_{sk}^{TE}J_s'\big(k_{c,sk}\rho\big)\sin(s\phi)\Big\} \quad (15)$$

and the transverse magnetic vector wave functions are obtained as follows,

$$\mathbf{h}_{sk}^{TM} = -\frac{j\omega\varepsilon_0}{k_{c,sk}^2}\hat{\mathbf{z}}\times\nabla_t e_{z,sk} = \frac{j\omega\varepsilon_0}{k_{c,sk}}\Big\{-\hat{\boldsymbol{\rho}}\frac{s}{k_{c,sk}\rho}\alpha_{sk}^{TM}J_s\big(k_{c,sk}\rho\big)\sin(s\phi) - \hat{\boldsymbol{\phi}}\alpha_{sk}^{TM}J_s'\big(k_{c,sk}\rho\big)\cos(s\phi)\Big\} \quad (16)$$

$$\mathbf{h}_{sk}^{TE} = -\frac{\gamma_{sk}}{k_{c,sk}^2}\nabla_t h_{z,sk} = \frac{\gamma_{sk}}{k_{c,sk}}\Big\{-\hat{\boldsymbol{\rho}}\alpha_{sk}^{TE}J_s'\big(k_{c,sk}\rho\big)\sin(s\phi) - \hat{\boldsymbol{\phi}}\frac{s}{k_{c,sk}\rho}\alpha_{sk}^{TE}J_s\big(k_{c,sk}\rho\big)\cos(s\phi)\Big\}, \quad (17)$$

where $J_s'(k_{c,sk}\rho) = \frac{\partial}{\partial(k_{c,sk}\rho)}J_s(k_{c,sk}\rho)$.

[22] The transverse electric and magnetic vector wave functions (14)–(17) are normalized by power,

$$\int_{S_w} \left(\mathbf{e}_{sk}^{TM,TE} \times \mathbf{h}_{sk}^{TM,TE}\right) \cdot \hat{\mathbf{z}} dS = 1, \tag{18}$$

where S_w is the waveguide cross section.

[23] The TE and TM cases are normalized separately resulting in the following expressions for the unknown coefficients. Thus for TM modes,

$$\alpha_{sk}^{TM} = \begin{cases} \dfrac{\sqrt{Z_{0k}^{TM}} k_{c,0k}/\gamma_{0k}}{a\sqrt{\pi\left[\left(J_2(k_{c,0k}a)\right)^2 - 2J_2(k_{c,0k}a)\dfrac{J_1(k_{c,0k}a)}{k_{c,0k}a} + \left(J_1(k_{c,0k}a)\right)^2\right]}}, & s = 0 \\ \dfrac{\sqrt{Z_{sk}^{TM}} k_{c,sk}/\gamma_{sk}}{a\sqrt{\dfrac{\pi}{2}} J_s'(k_{c,sk}a)}, & s \neq 0 \end{cases} \tag{19}$$

and for TE modes the coefficients are

$$\alpha_{sk}^{TE} = \begin{cases} \dfrac{k_{c,0k}/\gamma_{0k}}{a\sqrt{Z_{0k}^{TE}}\sqrt{\pi\left[\left(J_2(k_{c,0k}a)\right)^2 - 2J_2(k_{c,0k}a)\dfrac{J_1(k_{c,0k}a)}{k_{c,0k}a} + \left(J_1(k_{c,0k}a)\right)^2\right]}}, & s = 0 \\ \dfrac{k_{c,sk}/\gamma_{sk}}{a\sqrt{Z_{sk}^{TE}}\sqrt{\dfrac{\pi}{2}} J_s'(k_{c,sk}a)}, & s \neq 0, \end{cases} \tag{20}$$

where $Z_{sk}^{TM} = \frac{\gamma_{sk}}{j\omega\varepsilon_0}$ and $Z_{sk}^{TE} = \frac{j\omega\mu_0}{\gamma_{sk}}$ are the wave impedances of TM and TE modes, respectively.

[24] The coefficients given by (19) and (20) can be written in the form

$$\alpha_{sk}^{TM} = \frac{k_{c,sk}\sqrt{Z_{sk}^{TM}}}{\gamma_{sk}} c_{sk}, \alpha_{sk}^{TE} = \frac{k_{c,sk}}{\gamma_{sk}\sqrt{Z_{sk}^{TE}}} c_{sk}, \tag{21}$$

where

$$c_{sk} = \begin{cases} 1\Big/a\sqrt{\pi\left[\left(J_2(k_{c,0k}a)\right)^2 - 2J_2(k_{c,0k}a)\dfrac{J_1(k_{c,0k}a)}{k_{c,0k}a} + \left(J_1(k_{c,0k}a)\right)^2\right]}, & s = 0 \\ 1\Big/a\sqrt{\dfrac{\pi}{2}} J_s'(k_{c,sk}a), & s \neq 0. \end{cases} \tag{22}$$

[25] Following the same procedure for the other polarization, it can be easily shown that the coefficients β_{sk} are equal to α_{sk} for both TE and TM modes. Substituting (9) together with (12), (14), (15), and the corresponding expressions of the other polarization into the eigenmode expansion (7), we obtain the representation for the nine components of the electric dyadic Green's function of the ideal hard surface circular waveguide,

$$G_{\rho\rho}(\mathbf{r}, \mathbf{r}') = \frac{1}{2j\omega\mu_0} PV\Bigg\{ G_{\rho\rho}^{TEM} + \sum_{s=0}^{\infty}\sum_{k=1}^{\infty} c_{sk}^2 \cdot \Bigg\{ Z_{sk}^{TM} J_s'(k_{c,sk}\rho) J_s'(k_{c,sk}\rho') + \frac{s^2}{k_{c,sk}^2} Z_{sk}^{TE} \cdot \frac{J_s(k_{c,sk}\rho) J_s(k_{c,sk}\rho')}{\rho\rho'} \Bigg\} \cdot e^{-\gamma_{sk}|z-z'|} \cos(s(\phi - \phi')) \Bigg\} \tag{23}$$

$$G_{\rho\phi}(\mathbf{r}, \mathbf{r}') = \frac{1}{2j\omega\mu_0} PV\Bigg\{ G_{\rho\phi}^{TEM} + \sum_{s=0}^{\infty}\sum_{k=1}^{\infty} c_{sk}^2 s \cdot \Bigg\{ Z_{sk}^{TM} J_s'(k_{c,sk}\rho) \frac{J_s(k_{c,sk}\rho')}{k_{c,sk}\rho'} + Z_{sk}^{TE} \frac{J_s(k_{c,sk}\rho)}{k_{c,sk}\rho} \cdot J_s'(k_{c,sk}\rho') \Bigg\} e^{-\gamma_{sk}|z-z'|} \sin(s(\phi - \phi')) \Bigg\} \tag{24}$$

$$G_{\rho z}(\mathbf{r}, \mathbf{r}') = \frac{1}{2j\omega\mu_0} PV\Bigg\{ sign(z - z') \sum_{s=0}^{\infty}\sum_{k=1}^{\infty} c_{sk}^2 Z_{sk}^{TM} \frac{k_{c,sk}}{\gamma_{sk}} \cdot J_s'(k_{c,sk}\rho) J_s(k_{c,sk}\rho') \cdot e^{-\gamma_{sk}|z-z'|} \cos(s(\phi - \phi')) \Bigg\} \tag{25}$$

$$G_{\phi\rho}(\mathbf{r}, \mathbf{r}') = \frac{1}{2j\omega\mu_0} PV\Bigg\{ G_{\phi\rho}^{TEM} - \sum_{s=0}^{\infty}\sum_{k=1}^{\infty} c_{sk}^2 s \cdot \Bigg\{ Z_{sk}^{TM} J_s'(k_{c,sk}\rho') \frac{J_s(k_{c,sk}\rho)}{k_{c,sk}\rho} + Z_{sk}^{TE} \frac{J_s(k_{c,sk}\rho')}{k_{c,sk}\rho'} \cdot J_s'(k_{c,sk}\rho) \Bigg\} e^{-\gamma_{sk}|z-z'|} \sin(s(\phi - \phi')) \Bigg\} \tag{26}$$

$$G_{\phi\phi}(\mathbf{r}, \mathbf{r}') = \frac{1}{2j\omega\mu_0} PV\Bigg\{ G_{\phi\phi}^{TEM} + \sum_{s=0}^{\infty}\sum_{k=1}^{\infty} c_{sk}^2 \cdot \Bigg\{ \frac{s^2}{k_{c,sk}^2} Z_{sk}^{TM} \frac{J_s(k_{c,sk}\rho) J_s(k_{c,sk}\rho')}{\rho\rho'} + Z_{sk}^{TE} J_s'(k_{c,sk}\rho) J_s'(k_{c,sk}\rho') \Bigg\} \cdot e^{-\gamma_{sk}|z-z'|} \cos(s(\phi - \phi')) \Bigg\} \tag{27}$$

$$G_{\phi z}(\mathbf{r},\mathbf{r}') = -\frac{1}{2j\omega\mu_0} PV\left\{ sign(z-z') \sum_{s=0}^{\infty}\sum_{k=1}^{\infty} c_{sk}^2 Z_{sk}^{TM} \frac{s}{\gamma_{sk}} \cdot \frac{J_s(k_{c,sk}\rho)}{\rho} J_s(k_{c,sk}\rho') e^{-\gamma_{sk}|z-z'|} \cdot \sin(s(\phi-\phi')) \right\} \quad (28)$$

$$G_{z\rho}(\mathbf{r},\mathbf{r}') = -\frac{1}{2j\omega\mu_0} PV\left\{ sign(z-z') \sum_{s=0}^{\infty}\sum_{k=1}^{\infty} c_{sk}^2 Z_{sk}^{TM} \cdot \frac{k_{c,sk}}{\gamma_{sk}} J_s(k_{c,sk}\rho) J_s'(k_{c,sk}\rho') e^{-\gamma_{sk}|z-z'|} \cdot \cos(s(\phi-\phi')) \right\} \quad (29)$$

$$G_{z\phi}(\mathbf{r},\mathbf{r}') = -\frac{1}{2j\omega\mu_0} PV\left\{ sign(z-z') \sum_{s=0}^{\infty}\sum_{k=1}^{\infty} c_{sk}^2 Z_{sk}^{TM} \frac{s}{\gamma_{sk}} \cdot \frac{J_s(k_{c,sk}\rho')}{\rho'} J_s(k_{c,sk}\rho) e^{-\gamma_{sk}|z-z'|} \cdot \sin(s(\phi-\phi')) \right\} \quad (30)$$

$$G_{zz}(\mathbf{r},\mathbf{r}') = -\frac{1}{2j\omega\mu_0} PV\left\{ \sum_{s=0}^{\infty}\sum_{k=1}^{\infty} c_{sk}^2 Z_{sk}^{TM} \frac{k_{c,sk}^2}{\gamma_{sk}^2} J_s(k_{c,sk}\rho) \cdot J_s(k_{c,sk}\rho') e^{-\gamma_{sk}|z-z'|} \cos(s(\phi-\phi')) \right\} - \frac{\delta(\mathbf{r}-\mathbf{r}')}{k_0^2}. \quad (31)$$

[26] The TEM term included in expansion (7) of the dyadic Green's function is obtained in closed form as a contribution of TM and TE waveguide modes in the zero-cutoff limit, $k_{c,sk} \to 0$. It is shown below that the TEM part of the Green's function has only transverse components, $G_{\rho\rho}^{\mathrm{TEM}}$, $G_{\rho\phi}^{\mathrm{TEM}}$, $G_{\phi\rho}^{\mathrm{TEM}}$, and $G_{\phi\phi}^{\mathrm{TEM}}$.

[27] The zero-cutoff limit corresponds to the zero root of the characteristic equation (13) (except for $s = 0$, that is, $\lim_{k_{c,sk}\to 0} J_0(k_{c,sk}a) = 1$), which represents an additional solution in the series expansion of TM and TE modes associated with the TEM mode with the propagation constant $\gamma_0 = \lim_{k_{c,sk}\to 0} \gamma_{sk} = jk_0$.

[28] The transverse electric and magnetic vector wave functions of the TEM mode are obtained in the zero-cutoff limit of the corresponding expressions of TM and TE modes, (14)–(17),

$$\mathbf{e}_0^{TM} = jk_0 A^{TM} \lim_{k_{c,sk}\to 0} \left\{ -\hat{\boldsymbol{\rho}} J_s'(k_{c,sk}\rho)\cos(s\phi) + \hat{\boldsymbol{\phi}} s \frac{J_s(k_{c,sk}\rho)}{k_{c,sk}\rho}\sin(s\phi) \right\}$$

$$\mathbf{e}_0^{TE} = j\omega\mu_0 A^{TE} \lim_{k_{c,sk}\to 0} \left\{ -\hat{\boldsymbol{\rho}} s \frac{J_s(k_{c,sk}\rho)}{k_{c,sk}\rho}\cos(s\phi) + \hat{\boldsymbol{\phi}} J_s'(k_{c,sk}\rho)\sin(s\phi) \right\} \quad (32)$$

$$\mathbf{h}_0^{TM} = j\omega\varepsilon_0 A^{TM} \lim_{k_{c,sk}\to 0} \left\{ -\hat{\boldsymbol{\rho}} s \frac{J_s(k_{c,sk}\rho)}{k_{c,sk}\rho}\sin(s\phi) - \hat{\boldsymbol{\phi}} J_s'(k_{c,sk}\rho)\cos(s\phi) \right\}$$

$$\mathbf{h}_0^{TE} = jk_0 A^{TE} \lim_{k_{c,sk}\to 0} \left\{ -\hat{\boldsymbol{\rho}} J_s'(k_{c,sk}\rho)\sin(s\phi) - \hat{\boldsymbol{\phi}} s \frac{J_s(k_{c,sk}\rho)}{k_{c,sk}\rho}\cos(s\phi) \right\}, \quad (33)$$

where the coefficients A^{TM} and A^{TE} are defined as follows,

$$A^{TM} = \lim_{k_{c,sk}\to 0} \frac{\alpha_{sk}^{TM}}{k_{c,sk}} = \lim_{k_{c,sk}\to 0} \frac{c_{sk}\sqrt{Z_{sk}^{TM}}}{\gamma_{sk}} \quad (34)$$

$$A^{TE} = \lim_{k_{c,sk}\to 0} \frac{\alpha_{sk}^{TE}}{k_{c,sk}} = \lim_{k_{c,sk}\to 0} \frac{c_{sk}}{\gamma_{sk}\sqrt{Z_{sk}^{TE}}} = \lim_{k_{c,sk}\to 0} \frac{A^{TM}}{\sqrt{Z_{sk}^{TM} Z_{sk}^{TE}}} = \frac{A^{TM}}{\eta_0}, \quad (35)$$

with $\eta_0 = \sqrt{\frac{\mu_0}{\varepsilon_0}}$ being the intrinsic impedance of free space.

[29] Bessel functions and their derivatives in (32) and (33) are expanded in Taylor series,

$$J_s(k_{c,sk}\rho) = \frac{(k_{c,sk}\rho)^s}{2^s s!} - \frac{(k_{c,sk}\rho)^{s+2}}{2^{s+2}(s+1)!} + .. \quad (36)$$

$$J_s'(k_{c,sk}\rho) = \frac{(k_{c,sk}\rho)^{s-1}}{2^s (s-1)!} - \frac{(s+2)(k_{c,sk}\rho)^{s+1}}{2^{s+2}(s+1)!} + .., \quad (37)$$

which are used to find the limit of the following expressions,

$$\lim_{k_{c,sk}\to 0} \frac{J_s(k_{c,sk}\rho)}{k_{c,sk}\rho} = \begin{cases} 1/2, & s = 1 \\ 0, & s > 1 \end{cases} \quad (38)$$

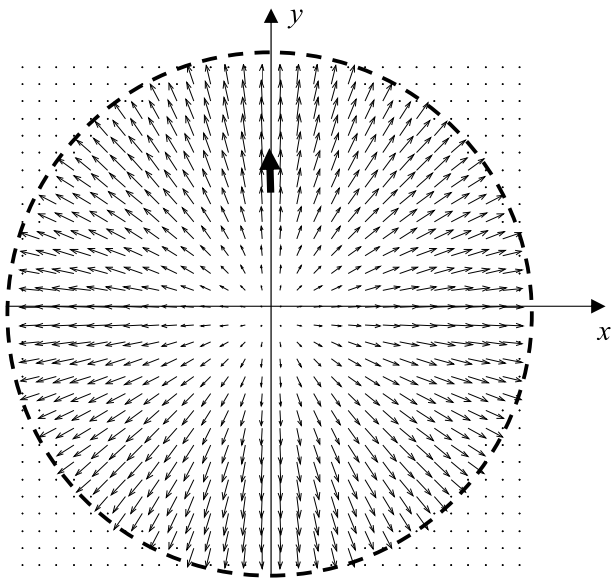

Figure 3. Transverse electric field of the TM_{01} mode plotted at $z = \lambda_g^{TM_{01}}/2 = 25.342$ mm due to the ρ-directed electric dipole at $z_0 = 0$ mm.

$$\lim_{k_{c,sk}\to 0} J_s'(k_{c,sk}\rho) = \begin{cases} 1/2, & s = 1 \\ 0, & s > 1. \end{cases} \tag{39}$$

[30] Taking into account (38) and (39) in expressions (32) and (33) we obtain the representation of electric and magnetic fields of the TEM mode (given in terms of TM and TE parts),

$$\begin{aligned} \mathbf{e}_0^{TM} &= \frac{1}{2} jk_0 A^{TM} \left\{ -\hat{\boldsymbol{\rho}} \cos(\phi) + \hat{\boldsymbol{\phi}} \sin(\phi) \right\} \\ \mathbf{e}_0^{TE} &= \frac{1}{2} j\omega\mu_0 \frac{A^{TM}}{\eta_0} \left\{ -\hat{\boldsymbol{\rho}} \cos(\phi) + \hat{\boldsymbol{\phi}} \sin(\phi) \right\} \end{aligned} \tag{40}$$

$$\begin{aligned} \mathbf{h}_0^{TM} &= \frac{1}{2} j\omega\varepsilon_0 A^{TM} \left\{ -\hat{\boldsymbol{\rho}} \sin(\phi) - \hat{\boldsymbol{\phi}} \cos(\phi) \right\} \\ \mathbf{h}_0^{TE} &= \frac{1}{2} jk_0 \frac{A^{TM}}{\eta_0} \left\{ -\hat{\boldsymbol{\rho}} \sin(\phi) - \hat{\boldsymbol{\phi}} \cos(\phi) \right\}, \end{aligned} \tag{41}$$

which are normalized by power,

$$\int_{S_w} \left(\left(\mathbf{e}_0^{TM} + \mathbf{e}_0^{TE} \right) \times \left(\mathbf{h}_0^{TM} + \mathbf{h}_0^{TE} \right) \right) \cdot \hat{\mathbf{z}} dS = 1, \tag{42}$$

resulting in the expression for A^{TM},

$$A^{TM} = \frac{1}{jk_0 a} \sqrt{\frac{\eta_0}{\pi}}. \tag{43}$$

[31] On the basis of the above derivations, the TEM term of the Green's function is obtained as the superposition of dyadic products of two orthogonal polarizations (sine and cosine angular solutions) of TM and TE modes in the zero-cutoff limit,

$$\begin{aligned} \overline{\mathbf{G}}^{TEM}(\phi, z; \phi', z') = PV \{ & \mathbf{e}_0^{TM,\cos}(\phi) \mathbf{e}_0^{TM,\cos}(\phi') \\ & + \mathbf{e}_0^{TM,\sin}(\phi) \mathbf{e}_0^{TM,\sin}(\phi') \\ & + \mathbf{e}_0^{TE,\cos}(\phi) \mathbf{e}_0^{TE,\cos}(\phi') \\ & + \mathbf{e}_0^{TE,\sin}(\phi) \mathbf{e}_0^{TE,\sin}(\phi') \} \; e^{-jk_0|z-z'|} \end{aligned} \tag{44}$$

or in terms of Green's function components,

$$\begin{aligned} G_{\rho\rho}^{TEM}(\phi, z; \phi', z') &= G_{\phi\phi}^{TEM}(\phi, z; \phi', z') \\ &= PV \frac{\eta_0}{2\pi a^2} \cos(\phi - \phi') e^{-jk_0|z-z'|} \end{aligned} \tag{45}$$

$$\begin{aligned} G_{\rho\phi}^{TEM}(\phi, z; \phi', z') &= -G_{\phi\rho}^{TEM}(\phi, z; \phi', z') \\ &= PV \frac{\eta_0}{2\pi a^2} \sin(\phi - \phi') e^{-jk_0|z-z'|}, \end{aligned} \tag{46}$$

which are included in the representations (23), (24), (26), and (27).

3. Excitation of Ideal Hard Surface Circular Waveguide Modes by an Electric Dipole Source

[32] The electric dyadic Green's function derived in the previous section has been used to obtain the electric field of representative TM, TE, and TEM modes excited in the ideal hard surface circular waveguide by an electric dipole source. Figures 3, 4, and 5 demonstrate the transverse electric field of TM_{01}, TE_{01}, and TEM modes at the distance of $z = \lambda_g/2$ (λ_g of the corresponding mode) from the source plane at $z_0 = 0$. The modes propagate in the ideal hard surface circular waveguide of radius $a = 11$ mm.

[33] Figure 3 shows the transverse electric field of the TM_{01} mode at 12 GHz due to the ρ-directed electric dipole source, $\mathbf{J}(\mathbf{r}) = \hat{\boldsymbol{\rho}} > \frac{1}{\rho}\delta(\rho - \frac{a}{2})\delta(\phi - \frac{\pi}{2})\delta(z)$. Obviously, the electric field distribution of this and, in general, all TM_{sk} modes is the same as in the PEC waveguide.

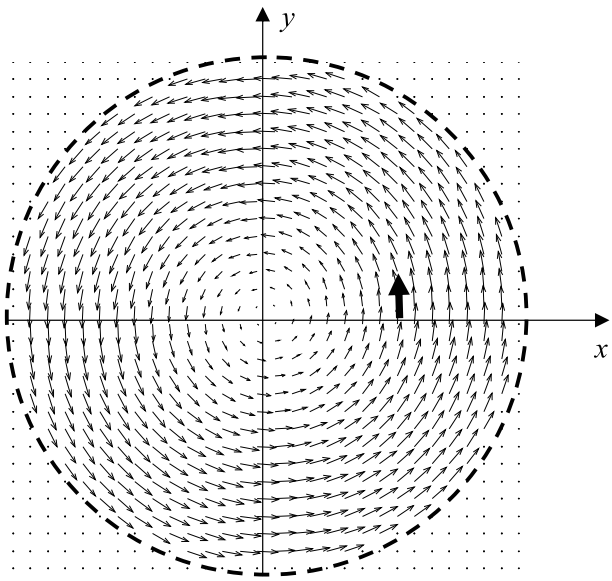

Figure 4. Transverse electric field of the TE_{01} mode plotted at $z = \lambda_g^{TE_{01}}/2 = 25.342$ mm due to the ϕ-directed electric dipole at $z_0 = 0$ mm.

[34] The transverse electric field of the TE_{01} mode at the same frequency due to the ϕ-directed electric dipole, $\mathbf{J}(\mathbf{r}) = \hat{\phi}\frac{1}{\rho}\delta(\rho - \frac{a}{2})\delta(\phi)\delta(z)$, is shown in Figure 4. It should be noted that the electric field of TE_{sk} modes propagating in the ideal hard surface waveguide (as in the PMC waveguide) is similar to the distribution of magnetic field of the corresponding TM_{sk} modes (propagating in the PEC waveguide).

[35] Figure 5 demonstrates the transverse electric field of the TEM mode at 10 GHz due to the ϕ-directed electric dipole, $\mathbf{J}(\mathbf{r}) = \hat{\phi}\frac{1}{\rho}\delta(\rho - \frac{a}{2})\delta(\phi - \frac{\pi}{4})\delta(z)$. It can be seen that the field is uniform over the waveguide cross section, and polarization of the field depends on polarization of the source. Clearly, the ideal hard surface circular waveguide supports a TEM mode polarized according to the orientation of the source.

4. Excitation of an Ideal Hard Surface Circular Waveguide by a Strip Dipole Antenna

[36] The Green's function derived in Section II is used in the method of moments analysis of hard surface waveguide excitation by a half-wavelength strip dipole antenna (with geometry shown in Figure 6). The dipole length is $2L = \lambda_0/2$ and dipole width is $2b = 0.25$ mm. The voltage delta gap source of 1 V is at the center of the dipole.

[37] The electric field integral equation for the current induced along the dipole (assuming only J_y component of the current for a thin strip dipole) is obtained by enforcing a boundary condition for the total tangential electric field,

$$-j\omega\mu_0\hat{\mathbf{y}}\cdot\int_{d-b}^{d+b}\int_{-L}^{L}\left\{\hat{\boldsymbol{\rho}}G_{\rho\rho}\hat{\boldsymbol{\rho}}' + \hat{\boldsymbol{\rho}}G_{\rho\phi}\hat{\boldsymbol{\phi}}' + \hat{\boldsymbol{\phi}}G_{\phi\rho}\hat{\boldsymbol{\rho}}' + \hat{\boldsymbol{\phi}}G_{\phi\phi}\hat{\boldsymbol{\phi}}'\right\}\cdot\hat{\mathbf{y}}'J_y(y')dy'dz' = -E_{gap}(y), \quad (47)$$

where the integral in the left-hand side of (47) is the electric field due to induced electric current and the right-hand side represents the excitation field. The electric dyadic Green's function used in this formulation has been derived for an ideal hard surface circular waveguide terminated with the PEC ground plane at $z = 0$ (with the Green's function components presented in Appendix A). The integral equation (47) is discretized via the method of moments with the piecewise-sinusoidal basis functions used for the current expansion (given in Appendix B). Galerkin's projection technique is used in the y direction along the strip and the delta function testing in the z direction across the strip. The method of moments impedance matrix elements are summarized in Appendix B.

[38] Convergence of the method of moments is studied for a different number of terms N used in the current expansion. The results shown in Figure 7 are obtained at

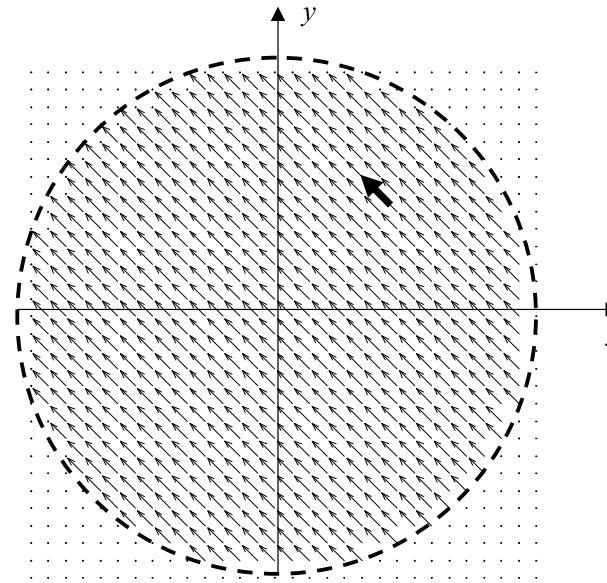

Figure 5. Transverse electric field of the TEM mode plotted at $z = \lambda_g^{TEM}/2 = 15$ mm due to the ϕ-directed electric dipole at $z_0 = 0$ mm.

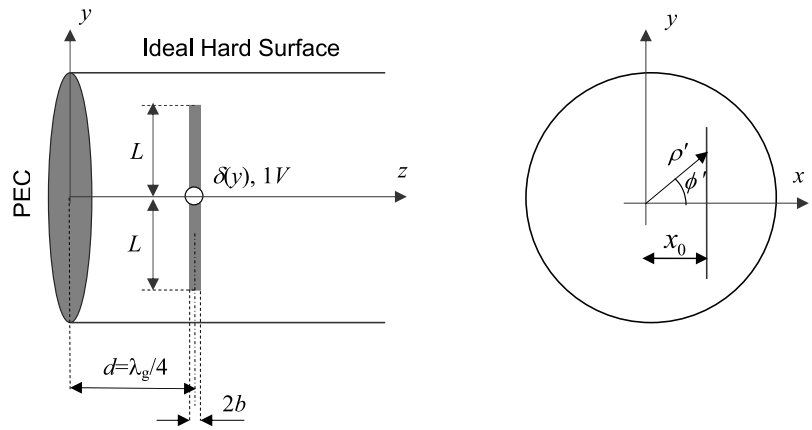

Figure 6. Half-wavelength strip dipole positioned at $\lambda_g/4$ from the PEC termination in the ideal hard surface circular waveguide. The dipole is shifted by an arbitrary distance x_0 from the waveguide axis.

10 GHz (λ_0 = 30 mm) for the half-wavelength strip dipole shifted at x_0 = 8 mm from the waveguide axis.

[39] The current behavior is studied with respect to the dipole position on the x axis as shown in Figure 8, where the current decreases as the dipole is shifted from the waveguide axis because of the interaction with the waveguide wall. The results presented in Figure 8 for real and imaginary part of the current are obtained at 10 GHz for a half-wavelength strip dipole, with 5 basis functions used in the current expansion.

[40] The electric field of the TEM mode excited by the strip dipole at 10 GHz is obtained by integrating the four transverse components of the TEM term of the Green's function with the current obtained from the method of

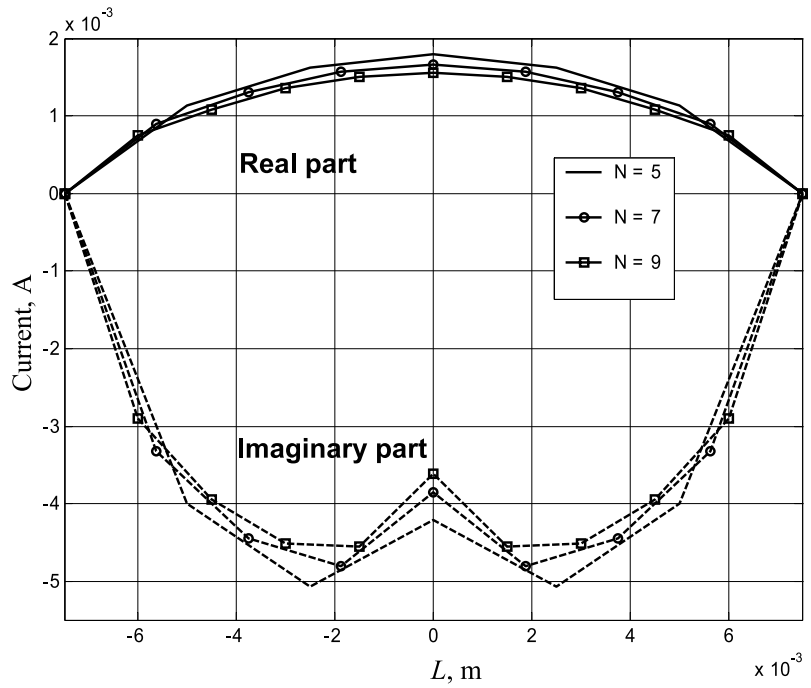

Figure 7. Behavior of the strip dipole current (real and imaginary parts) for a different number of piecewise-sinusoidal basis functions N used in the current expansion.

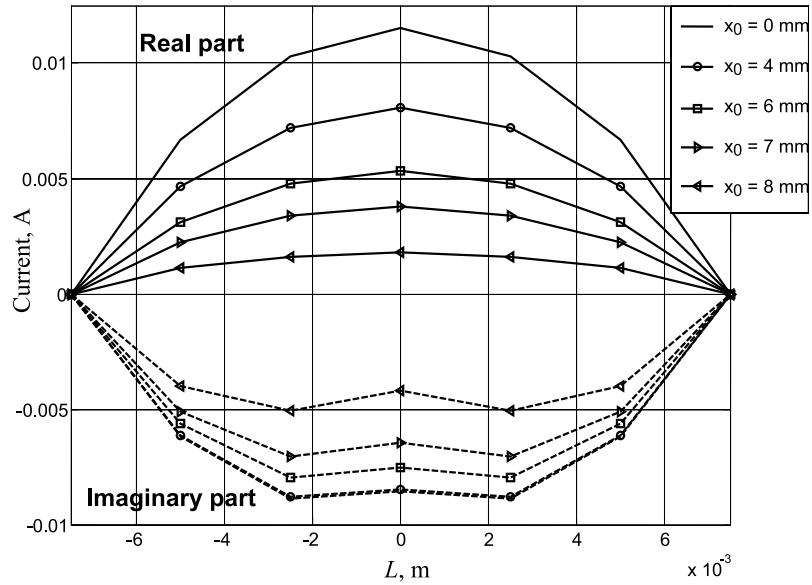

Figure 8. Behavior of the strip dipole current (real and imaginary parts) with respect to the dipole position on the x axis.

moments solution (since all the other modes are evanescent in the hard surface waveguide at this frequency),

$$\mathbf{E}(\mathbf{r}) = -j\omega\mu_0 \sum_{n=1}^{N} I_n \int_{y_n-\Delta y}^{y_n+\Delta y} \left\{ \hat{\boldsymbol{\rho}} G_{\rho\rho}^{TEM} \hat{\boldsymbol{\rho}}' + \hat{\boldsymbol{\rho}} G_{\rho\phi}^{TEM} \hat{\boldsymbol{\phi}}' + \hat{\boldsymbol{\phi}} G_{\phi\rho}^{TEM} \hat{\boldsymbol{\rho}}' + \hat{\boldsymbol{\phi}} G_{\phi\phi}^{TEM} \hat{\boldsymbol{\phi}}' \right\} \cdot \hat{\mathbf{y}}' S_n(y') dy'. \quad (48)$$

[41] The results of the TEM mode excitation by a half-wavelength strip dipole in the ideal hard surface circular waveguide of radius a = 11 mm at the frequency f = 10 GHz are shown in Figure 9.

5. Scattering of the TEM Mode by Thin Strip in the Ideal Hard Surface Waveguide

[42] The Green's function derived in Section II is used in the method of moments analysis of scattering of the TEM mode by a thin metal strip arbitrarily positioned in the ideal hard surface circular waveguide as shown in Figure 10. The strip width is $2w$ = 0.25 mm, strip length is $2h$ = 15 mm, and the radius of waveguide is a = 11 mm. The l component of the incident electric field of the TEM mode is obtained as follows,

$$E_l^{inc}(\phi, z) = \frac{1}{2a}\sqrt{\frac{\eta_0}{\pi}}\left(\hat{\mathbf{l}} \cdot \hat{\boldsymbol{\rho}} \cos(\phi) + \hat{\mathbf{l}} \cdot \hat{\boldsymbol{\phi}} \sin(\phi)\right) e^{-jk_0 z}, \quad (49)$$

where $\hat{\mathbf{l}} = \hat{\mathbf{x}}\cos(\alpha) + \hat{\mathbf{y}}\sin(\alpha)$.

[43] The scattered electric field tangential to the strip is calculated using the four components of the ideal hard surface Green's function, (23), (24), (26), and (27),

$$E_l^{sc}(\mathbf{r}) = -j\omega\mu_0 \hat{\mathbf{l}} \cdot \int_{-w}^{w} \int_{-h}^{h} \left\{ \hat{\boldsymbol{\rho}} G_{\rho\rho} \hat{\boldsymbol{\rho}}' + \hat{\boldsymbol{\rho}} G_{\rho\phi} \hat{\boldsymbol{\phi}}' + \hat{\boldsymbol{\phi}} G_{\phi\rho} \hat{\boldsymbol{\rho}}' + \hat{\boldsymbol{\phi}} G_{\phi\phi} \hat{\boldsymbol{\phi}}' \right\} \cdot \hat{\mathbf{l}}' J(l') dl' dz'. \quad (50)$$

[44] The electric field integral equation is obtained by enforcing the boundary condition for the total tangential electric field on the surface of the strip, which is discretized via the method of moments. The current is expanded in terms of piecewise-sinusoidal basis functions in the l direction given in Appendix B. Galerkin's projection technique is applied for testing in the l coordinate and the delta function is used for testing in the z coordinate. The method of moments impedance matrix is summarized in Appendix C.

[45] The scattered electric field at the distance $d = \lambda_0$ from the strip is calculated as the integral of the TEM term of the Green's function with the current obtained from the method of moments solution (assuming all the other modes are evanescent in the ideal hard surface waveguide at the operating frequency),

$$\mathbf{E}^{sc}(\mathbf{r}) = -j\omega\mu_0 \sum_{n=1}^{N} I_n \int_{l_n-\Delta l}^{l_n+\Delta l} \left\{ \hat{\boldsymbol{\rho}} G_{\rho\rho}^{TEM} \hat{\boldsymbol{\rho}}' + \hat{\boldsymbol{\rho}} G_{\rho\phi}^{TEM} \hat{\boldsymbol{\phi}}' + \hat{\boldsymbol{\phi}} G_{\phi\rho}^{TEM} \hat{\boldsymbol{\rho}}' + \hat{\boldsymbol{\phi}} G_{\phi\phi}^{TEM} \hat{\boldsymbol{\phi}}' \right\} \cdot \hat{\mathbf{l}}' S_n(l') dl'. \quad (51)$$

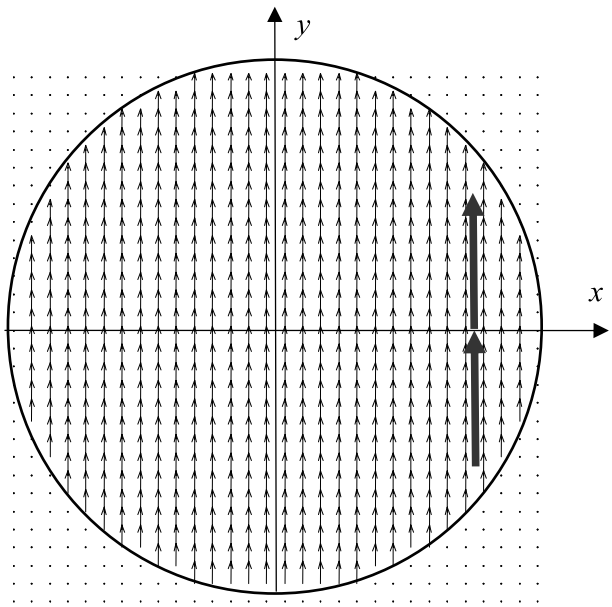

Figure 9. Field distribution of the TEM mode excited by a half-wavelength strip dipole shifted at $x_0 = 8$ mm from the waveguide axis in the ideal hard surface circular waveguide terminated with the PEC ground plane.

[46] The reflection coefficient at port 1 with coordinates $(a/2, 0, -d)$ is defined as the ratio of the scattered field over the incident field,

$$S_{11} = \frac{E_\phi^{sc}(a/2,\ 0,\ -d)}{E_\phi^{inc}(a/2,\ 0,\ -d)}, \tag{52}$$

and the transmission coefficient is defined as the ratio of the total field at port 2 with coordinates $(a/2, 0, d)$ over the incident field at port 1,

$$S_{21} = \frac{E_\phi^{sc}(a/2,\ 0,\ d) + E_\phi^{inc}(a/2,\ 0,\ d)}{E_\phi^{inc}(a/2,\ 0,\ -d)}. \tag{53}$$

[47] The realistic hard surface was modeled using the finite difference time domain commercial software Quick Wave [*QWED*, 1998] by placing 180 longitudinal metal strips of azimuthal width $w = 1^\circ$ inside the dielectric coating with the inner radius $a = 11$ mm, dielectric permittivity $\varepsilon_r = 2.2$, and thickness $t = 6.8$ mm calculated as a quarter of the effective wavelength,

$$t = \frac{\lambda_0}{4\sqrt{\varepsilon_r - 1}}. \tag{54}$$

[48] The reflection and transmission coefficients for the strip in the ideal hard surface waveguide calculated using (52) and (53) compared to the scattering parameters obtained using Quick Wave [*QWED*, 1998] for the realistic hard surface are shown in Figure 11. In the method of moments code, the number of basis functions used is 5 and the number of terms in the Green's function expansion is 40×40.

6. Conclusion

[49] The Green's function analysis of ideal hard surface circular waveguide is based on the decomposition of the structure into PEC and PMC waveguides. The electric Green's dyadic due to an arbitrarily oriented electric dipole source is obtained in terms of solenoidal and irrotational parts. The solenoidal part is expressed by the eigenmode expansion of TM and TE modes of the PEC and PMC circular waveguides, respectively, with an additional term associated with the TEM mode. The TEM term of the Green's dyadic is obtained in closed form as a contribution of TM and TE modes in the zero-cutoff limit. It is shown that the TEM mode of the ideal hard surface circular waveguide has a uniform field distribution over the waveguide cross section, and polarization of the mode necessarily depends on polarization of the electric dipole source. The Green's function of an ideal hard

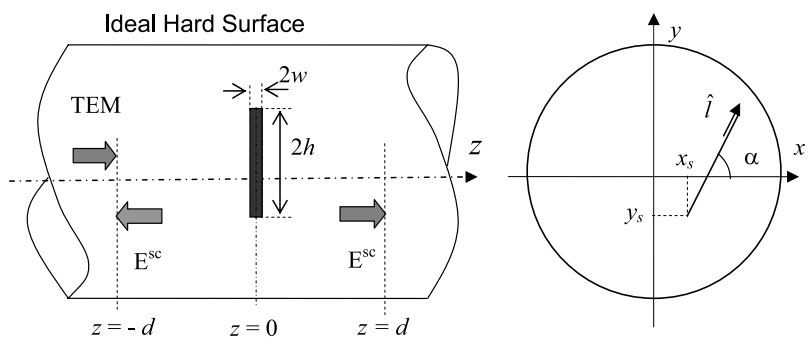

Figure 10. Geometry of the ideal hard surface circular waveguide with an arbitrarily positioned l-directed thin metal strip. The strip has a fixed point at (x_s, y_s).

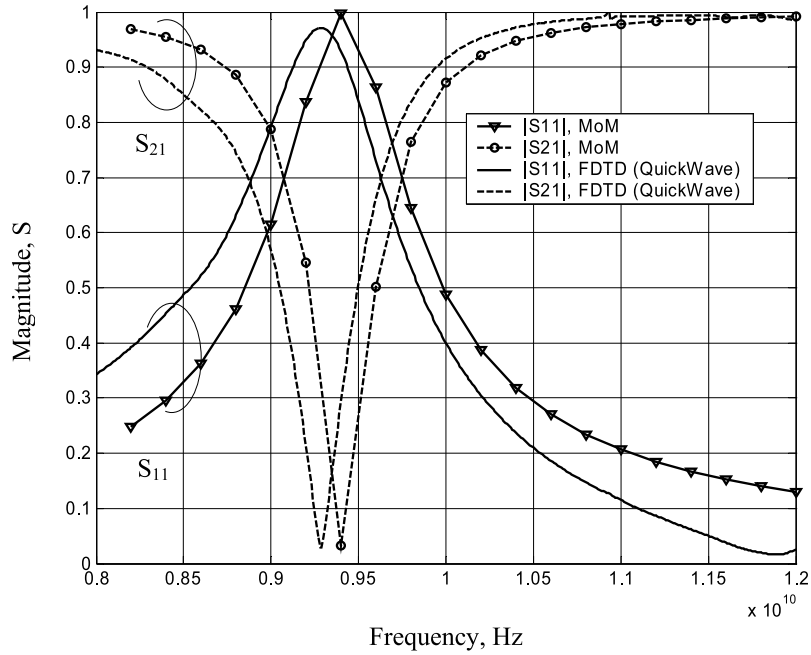

Figure 11. Scattering parameters for the strip in the ideal hard surface waveguide obtained from the method of moments solution and compared with the finite difference time domain simulation for the same strip in the realistic hard surface.

surface circular waveguide terminated with the PEC ground plane has been used in the method of moments analysis of the waveguide excitation by a half-wavelength strip dipole antenna. In addition, scattering of the TEM mode in the ideal hard surface waveguide has been analyzed on the basis of the method of moments and the Green's function derived in this work.

Appendix A: Dyadic Green's Function for Semi-Infinite Waveguide

[50] The Green's function components of an ideal hard surface circular waveguide terminated with the PEC ground plane at $z = 0$ are summarized as follows,

$$G_{\rho\rho}(\mathbf{r},\ \mathbf{r}') = \frac{1}{j\omega\mu_0} PV\left\{ \frac{\eta_0}{2\pi a^2} f_0(z,\ z') \cos(\phi - \phi') + \sum_{s=0}^{\infty}\sum_{k=1}^{\infty} c_{sk}^2 \left\{ Z_{sk}^{TM} J_s'\left(k_{c,sk}\rho\right) J_s'\left(k_{c,sk}\rho'\right) + \frac{s^2}{k_{c,sk}^2} Z_{sk}^{TE} \frac{J_s\left(k_{c,sk}\rho\right) J_s\left(k_{c,sk}\rho'\right)}{\rho\rho'} \right\} \cdot f_{sk}(z,z') \cos(s(\phi - \phi')) \right\} \tag{A1}$$

$$G_{\rho\phi}(\mathbf{r},\ \mathbf{r}') = \frac{1}{j\omega\mu_0} PV\left\{ \frac{\eta_0}{2\pi a^2} f_0(z,z') \sin(\phi - \phi') + \sum_{s=0}^{\infty}\sum_{k=1}^{\infty} c_{sk}^2 s \left\{ Z_{sk}^{TM} J_s'\left(k_{c,sk}\rho\right) \frac{J_s\left(k_{c,sk}\rho'\right)}{k_{c,sk}\rho'} + Z_{sk}^{TE} \frac{J_s\left(k_{c,sk}\rho\right)}{k_{c,sk}\rho} J_s'\left(k_{c,sk}\rho'\right) \right\} \cdot f_{sk}(z,z') \sin(s(\phi - \phi')) \right\} \tag{A2}$$

$$G_{\rho z}(\mathbf{r},\ \mathbf{r}') = \frac{1}{j\omega\mu_0} PV\left\{ sign(z - z') \sum_{s=0}^{\infty}\sum_{k=1}^{\infty} c_{sk}^2 Z_{sk}^{TM} \frac{k_{c,sk}}{\gamma_{sk}} \cdot J_s'\left(k_{c,sk}\rho\right) J_s\left(k_{c,sk}\rho'\right) g_{sk}(z,z') \cdot \cos(s(\phi - \phi')) \right\} \tag{A3}$$

$$G_{\phi\rho}(\mathbf{r},\ \mathbf{r}') = -\frac{1}{j\omega\mu_0} PV\left\{ \frac{\eta_0}{2\pi a^2} f_0(z,z') \sin(\phi - \phi') + \sum_{s=0}^{\infty}\sum_{k=1}^{\infty} c_{sk}^2 s \left\{ Z_{sk}^{TM} J_s'\left(k_{c,sk}\rho'\right) \frac{J_s\left(k_{c,sk}\rho\right)}{k_{c,sk}\rho} + Z_{sk}^{TE} \frac{J_s\left(k_{c,sk}\rho'\right)}{k_{c,sk}\rho'} J_s'\left(k_{c,sk}\rho\right) \right\} \cdot f_{sk}(z,z') \sin(s(\phi - \phi')) \right\} \tag{A4}$$

$$G_{\phi\phi}(\mathbf{r},\mathbf{r}') = \frac{1}{j\omega\mu_0} PV\Bigg\{ \frac{\eta_0}{2\pi a^2} f_0(z,z')\cos(\phi-\phi') + \sum_{s=0}^{\infty}\sum_{k=1}^{\infty} c_{sk}^2 \Bigg\{ \frac{s^2}{k_{c,sk}^2} Z_{sk}^{TM} \frac{J_s(k_{c,sk}\rho) J_s(k_{c,sk}\rho')}{\rho\rho'} + Z_{sk}^{TE} J_s'(k_{c,sk}\rho) J_s'(k_{c,sk}\rho') \Bigg\} \cdot f_{sk}(z,z')\cos(s(\phi-\phi')) \Bigg\} \tag{A5}$$

$$G_{\phi z}(\mathbf{r},\mathbf{r}') = -\frac{1}{j\omega\mu_0} PV\Bigg\{ sign(z-z') \sum_{s=0}^{\infty}\sum_{k=1}^{\infty} c_{sk}^2 Z_{sk}^{TM} \frac{s}{\gamma_{sk}} \cdot \frac{J_s(k_{c,sk}\rho)}{\rho} J_s(k_{c,sk}\rho') g_{sk}(z,z') \cdot \sin(s(\phi-\phi')) \Bigg\} \tag{A6}$$

$$G_{z\rho}(\mathbf{r},\mathbf{r}') = -\frac{1}{j\omega\mu_0} PV\Bigg\{ sign(z-z') \sum_{s=0}^{\infty}\sum_{k=1}^{\infty} c_{sk}^2 Z_{sk}^{TM} \frac{k_{c,sk}}{\gamma_{sk}} \cdot J_s(k_{c,sk}\rho) J_s'(k_{c,sk}\rho') g_{sk}(z,z') \cdot \cos(s(\phi-\phi')) \Bigg\} \tag{A7}$$

$$G_{z\phi}(\mathbf{r},\mathbf{r}') = -\frac{1}{j\omega\mu_0} PV\Bigg\{ sign(z-z') \sum_{s=0}^{\infty}\sum_{k=1}^{\infty} c_{sk}^2 Z_{sk}^{TM} \frac{s}{\gamma_{sk}} \cdot \frac{J_s(k_{c,sk}\rho')}{\rho'} J_s(k_{c,sk}\rho) g_{sk}(z,z') \cdot \sin(s(\phi-\phi')) \Bigg\} \tag{A8}$$

$$G_{zz}(\mathbf{r},\mathbf{r}') = -\frac{1}{j\omega\mu_0} PV\Bigg\{ \sum_{s=0}^{\infty}\sum_{k=1}^{\infty} c_{sk}^2 Z_{sk}^{TM} \frac{k_{c,sk}^2}{\gamma_{sk}^2} J_s(k_{c,sk}\rho) \cdot J_s(k_{c,sk}\rho')\, g_{sk}(z,z')\cos(s(\phi-\phi')) \Bigg\} - \frac{\delta(\mathbf{r}-\mathbf{r}')}{k_0^2}, \tag{A9}$$

where

$$f_{sk}(z,z') = \begin{cases} e^{-\gamma_{sk}z}\sinh(\gamma_{sk}z'), & z \geq z' \\ e^{-\gamma_{sk}z'}\sinh(\gamma_{sk}z), & z < z' \end{cases} \tag{A10}$$

$$g_{sk}(z,z') = \begin{cases} e^{-\gamma_{sk}z}\cosh(\gamma_{sk}z'), & z \geq z' \\ e^{-\gamma_{sk}z'}\cosh(\gamma_{sk}z), & z < z' \end{cases} \tag{A11}$$

$$f_0(z,z') = \begin{cases} je^{-jk_0z}\sin(k_0z'), & z \geq z' \\ je^{-jk_0z'}\sin(k_0z), & z < z'. \end{cases} \tag{A12}$$

Appendix B: Method of Moments (MOM) Impedance Matrix for Strip Dipole Antenna

[51] Piecewise-sinusoidal basis functions used in the current expansion are

$$S_n(y') = \begin{cases} \dfrac{\sin(k_0(y'-y_n+\Delta y))}{\sin(k_0\Delta y)}, & y_{n-1} \leq y' \leq y_n \\ \dfrac{\sin(k_0(y_n+\Delta y-y'))}{\sin(k_0\Delta y)}, & y_n \leq y' \leq y_{n+1} \\ 0, & \text{otherwise.} \end{cases} \tag{B1}$$

[52] The method of moments impedance matrix elements obtained in the discretization of integral equation (47) are

$$\begin{aligned} Z_{mn} = {} & \frac{1}{4bjk_0\pi a^2}\frac{\eta_0}{}\zeta_0 \int_{y_m-\Delta y}^{y_m+\Delta y}\int_{y_n-\Delta y}^{y_n+\Delta y} S_n(y')S_m(y) \cdot (\xi_1^{css}(y,y') + \xi_1^{ssc}(y,y') + \xi_1^{scs}(y,y') + \xi_1^{ccc}(y,y'))dy'dy + \frac{1}{2b}\sum_{s=0}^{\infty}\sum_{k=1}^{\infty} c_{sk}^2\zeta_{sk}\Bigg\{ Z_{sk}^{TM} \cdot \Bigg[\int_{y_m-\Delta y}^{y_m+\Delta y}\int_{y_n-\Delta y}^{y_n+\Delta y} J_s'(k_{c,sk}\rho_0)J_s'(k_{c,sk}\rho_0')S_n(y') \cdot S_m(y)\xi_s^{css}(y,y')dy'dy + \frac{s}{k_{c,sk}}\int_{y_m-\Delta y}^{y_m+\Delta y}\int_{y_n-\Delta y}^{y_n+\Delta y} \cdot J_s'(k_{c,sk}\rho_0)\frac{J_s(k_{c,sk}\rho_0')}{\rho_0'}S_n(y')S_m(y)\xi_s^{ssc}(y,y')dy'dy \\ & - \frac{s}{k_{c,sk}}\int_{y_m-\Delta y}^{y_m+\Delta y}\int_{y_n-\Delta y}^{y_n+\Delta y} J_s'(k_{c,sk}\rho_0')\frac{J_s(k_{c,sk}\rho_0)}{\rho_0} \cdot S_n(y')S_m(y)\xi_s^{scs}(y,y')dy'dy + \frac{s^2}{k_{c,sk}^2}\int_{y_m-\Delta y}^{y_m+\Delta y} \cdot \int_{y_n-\Delta y}^{y_n+\Delta y}\frac{J_s(k_{c,sk}\rho_0)}{\rho_0}\frac{J_s(k_{c,sk}\rho_0')}{\rho_0'}S_n(y')S_m(y)\xi_s^{ccc}(y,y') \cdot dy'dy\Bigg] + Z_{sk}^{TE}\Bigg[\int_{y_m-\Delta y}^{y_m+\Delta y}\int_{y_n-\Delta y}^{y_n+\Delta y} J_s'(k_{c,sk}\rho_0) \cdot J_s'(k_{c,sk}\rho_0')S_n(y')S_m(y)\xi_s^{ccc}(y,y')dy'dy - \frac{s}{k_{c,sk}} \cdot \int_{y_m-\Delta y}^{y_m+\Delta y}\int_{y_n-\Delta y}^{y_n+\Delta y} J_s'(k_{c,sk}\rho_0)\frac{J_s(k_{c,sk}\rho_0')}{\rho_0'}S_n(y') \cdot S_m(y)\xi_s^{scs}(y,y')dy'dy + \frac{s}{k_{c,sk}}\int_{y_m-\Delta y}^{y_m+\Delta y}\int_{y_n-\Delta y}^{y_n+\Delta y} \cdot J_s'(k_{c,sk}\rho_0')\frac{J_s(k_{c,sk}\rho_0)}{\rho_0}S_n(y')S_m(y)\xi_s^{ssc}(y,y')dy'dy \\ & + \frac{s^2}{k_{c,sk}^2}\int_{y_m-\Delta y}^{y_m+\Delta y}\int_{y_n-\Delta y}^{y_n+\Delta y}\frac{J_s(k_{c,sk}\rho_0)}{\rho_0}\frac{J_s(k_{c,sk}\rho_0')}{\rho_0'} \cdot S_n(y')S_m(y)\xi_s^{css}(y,y')dy'dy\Bigg]\Bigg\}, \end{aligned} \tag{B2}$$

where

$$\rho_0 = \sqrt{x_0^2 + y^2}, \quad \rho_0' = \sqrt{x_0^2 + y'^2}$$

$$\begin{aligned}
\xi_1^{css}(y,y') &= \cos\left(\tan^{-1}(y/x_0) - \tan^{-1}(y'/x_0)\right) \\
&\quad \cdot \sin\left(\tan^{-1}(y/x_0)\right)\sin\left(\tan^{-1}(y'/x_0)\right) \\
\xi_1^{ssc}(y,y') &= \sin\left(\tan^{-1}(y/x_0) - \tan^{-1}(y'/x_0)\right) \\
&\quad \cdot \sin\left(\tan^{-1}(y/x_0)\right)\cos\left(\tan^{-1}(y'/x_0)\right) \\
\xi_1^{scs}(y,y') &= \sin\left(\tan^{-1}(y/x_0) - \tan^{-1}(y'/x_0)\right) \\
&\quad \cdot \cos\left(\tan^{-1}(y/x_0)\right)\sin\left(\tan^{-1}(y'/x_0)\right) \\
\xi_1^{ccc}(y,y') &= \cos\left(\tan^{-1}(y/x_0) - \tan^{-1}(y'/x_0)\right) \\
&\quad \cdot \cos\left(\tan^{-1}(y/x_0)\right)\cos\left(\tan^{-1}(y'/x_0)\right) \\
\xi_s^{css}(y,y') &= \cos\left[s\left(\tan^{-1}(y/x_0) - \tan^{-1}(y'/x_0)\right)\right] \\
&\quad \cdot \sin\left(\tan^{-1}(y/x_0)\right)\sin\left(\tan^{-1}(y'/x_0)\right) \\
\xi_s^{ssc}(y,y') &= \sin\left[s\left(\tan^{-1}(y/x_0) - \tan^{-1}(y'/x_0)\right)\right] \\
&\quad \cdot \sin\left(\tan^{-1}(y/x_0)\right)\cos\left(\tan^{-1}(y'/x_0)\right) \\
\xi_s^{scs}(y,y') &= \sin\left[s\left(\tan^{-1}(y/x_0) - \tan^{-1}(y'/x_0)\right)\right] \\
&\quad \cdot \cos\left(\tan^{-1}(y/x_0)\right)\sin\left(\tan^{-1}(y'/x_0)\right) \\
\xi_s^{ccc}(y,y') &= \cos\left[s\left(\tan^{-1}(y/x_0) - \tan^{-1}(y'/x_0)\right)\right] \\
&\quad \cdot \cos\left(\tan^{-1}(y/x_0)\right)\cos\left(\tan^{-1}(y'/x_0)\right) \qquad \text{(B3)}
\end{aligned}$$

and

$$\begin{aligned}
\zeta_0 &= \frac{1}{jk_0}\left(1 - e^{-jk_0 b} + \frac{e^{-j2k_0 d}}{2}\left(e^{-jk_0 b} - e^{jk_0 b}\right)\right) \\
\zeta_{sk} &= \frac{1}{\gamma_{sk}}\left(1 - e^{-\gamma_{sk} b} + \frac{e^{-2\gamma_{sk} d}}{2}\left(e^{-\gamma_{sk} b} - e^{\gamma_{sk} b}\right)\right). \qquad \text{(B4)}
\end{aligned}$$

Appendix C: MOM Impedance Matrix for Strip Scatterer

[53] Method of moments impedance matrix elements obtained in the analysis of scattering of the TEM mode by a thin strip arbitrarily positioned in the ideal hard surface circular waveguide are summarized as follows:

$$\begin{aligned}
Z_{mn} = {} & \frac{\eta_0}{4w\pi a^2}\frac{1 - e^{-jk_0 w}}{jk_0}\int_{l_m-\Delta l}^{l_m+\Delta l}\int_{l_n-\Delta l}^{l_n+\Delta l} S_n(l')S_m(l) \\
& \cdot \left(\xi_1^{ccc}(l,l') + \xi_1^{scs}(l,l') + \xi_1^{ssc}(l,l') + \xi_1^{css}(l,l')\right) \\
& \cdot dl'dl + \frac{1}{2w}\sum_{s=0}^{\infty}\sum_{k=1}^{\infty} c_{sk}^2 \frac{1 - e^{-\gamma_{sk} w}}{\gamma_{sk}}\left\{ Z_{sk}^{TM}\left[\int_{l_m-\Delta l}^{l_m+\Delta l}\right.\right. \\
& \cdot \int_{l_n-\Delta l}^{l_n+\Delta l} J_s'\left(k_{c,sk}\rho\right)J_s'\left(k_{c,sk}\rho'\right)S_n(l')S_m(l)\xi_s^{ccc}(l,l') \\
& \cdot dl'dl + \frac{s}{k_{c,sk}}\int_{l_m-\Delta l}^{l_m+\Delta l}\int_{l_n-\Delta l}^{l_n+\Delta l} J_s'\left(k_{c,sk}\rho\right)\frac{J_s\left(k_{c,sk}\rho'\right)}{\rho'} \\
& \cdot S_n(l')S_m(l)\xi_s^{scs}(l,l')dl'dl - \frac{s}{k_{c,sk}}\int_{l_m-\Delta l}^{l_m+\Delta l}\int_{l_n-\Delta l}^{l_n+\Delta l} \\
& \cdot J_s'\left(k_{c,sk}\rho'\right)\frac{J_s\left(k_{c,sk}\rho\right)}{\rho} S_n(l')S_m(l)\xi_s^{ssc}(l,l')dl'dl \\
& + \frac{s^2}{k_{c,sk}^2}\int_{l_m-\Delta l}^{l_m+\Delta l}\int_{l_n-\Delta l}^{l_n+\Delta l}\frac{J_s\left(k_{c,sk}\rho\right)}{\rho}\frac{J_s\left(k_{c,sk}\rho'\right)}{\rho'}S_n(l') \\
& \cdot S_m(l)\xi_s^{css}(l,l')dl'dl\Big] + Z_{sk}^{TE}\left[\int_{l_m-\Delta l}^{l_m+\Delta l}\int_{l_n-\Delta l}^{l_n+\Delta l}\right. \\
& \cdot J_s'\left(k_{c,sk}\rho\right)J_s'\left(k_{c,sk}\rho'\right)S_n(l')S_m(l)\xi_s^{css}(l,l')dl'dl \\
& - \frac{s}{k_{c,sk}}\int_{l_m-\Delta l}^{l_m+\Delta l}\int_{l_n-\Delta l}^{l_n+\Delta l} J_s'\left(k_{c,sk}\rho\right)\frac{J_s\left(k_{c,sk}\rho'\right)}{\rho'}S_n(l') \\
& \cdot S_m(l)\xi_s^{ssc}(l,l')dl'dl + \frac{s}{k_{c,sk}}\int_{l_m-\Delta l}^{l_m+\Delta l}\int_{l_n-\Delta l}^{l_n+\Delta l} \\
& \cdot J_s'\left(k_{c,sk}\rho'\right)\frac{J_s\left(k_{c,sk}\rho\right)}{\rho} S_n(l')S_m(l)\xi_s^{scs}(l,l')dl'dl \\
& + \frac{s^2}{k_{c,sk}^2}\int_{l_m-\Delta l}^{l_m+\Delta l}\int_{l_n-\Delta l}^{l_n+\Delta l}\frac{J_s\left(k_{c,sk}\rho\right)}{\rho}\frac{J_s\left(k_{c,sk}\rho'\right)}{\rho'}S_n(l') \\
& \cdot S_m(l)\xi_s^{ccc}(l,l')dl'dl\Big]\Big\}, \qquad \text{(C1)}
\end{aligned}$$

where

$$\begin{aligned}
\xi_1^{ccc}(l,l') &= \cos\left(\tan^{-1}(y/x) - \tan^{-1}(y'/x')\right) \\
&\quad \cdot \cos\left(\alpha - \tan^{-1}(y/x)\right)\cos\left(\alpha - \tan^{-1}(y'/x')\right) \\
\xi_1^{scs}(l,l') &= \sin\left(\tan^{-1}(y/x) - \tan^{-1}(y'/x')\right) \\
&\quad \cdot \cos\left(\alpha - \tan^{-1}(y/x)\right)\sin\left(\alpha - \tan^{-1}(y'/x')\right) \\
\xi_1^{ssc}(l,l') &= \sin\left(\tan^{-1}(y/x) - \tan^{-1}(y'/x')\right) \\
&\quad \cdot \sin\left(\alpha - \tan^{-1}(y/x)\right)\cos\left(\alpha - \tan^{-1}(y'/x')\right) \\
\xi_1^{css}(l,l') &= \cos\left(\tan^{-1}(y/x) - \tan^{-1}(y'/x')\right) \\
&\quad \cdot \sin\left(\alpha - \tan^{-1}(y/x)\right)\sin\left(\alpha - \tan^{-1}(y'/x')\right) \\
\xi_s^{ccc}(l,l') &= \cos\left[s\left(\tan^{-1}(y/x) - \tan^{-1}(y'/x')\right)\right] \\
&\quad \cdot \cos\left(\alpha - \tan^{-1}(y/x)\right)\cos\left(\alpha - \tan^{-1}(y'/x')\right) \\
\xi_s^{scs}(l,l') &= \sin\left[s\left(\tan^{-1}(y/x) - \tan^{-1}(y'/x')\right)\right] \\
&\quad \cdot \cos\left(\alpha - \tan^{-1}(y/x)\right)\sin\left(\alpha - \tan^{-1}(y'/x')\right) \\
\xi_s^{ssc}(l,l') &= \sin\left[s\left(\tan^{-1}(y/x) - \tan^{-1}(y'/x')\right)\right] \\
&\quad \cdot \sin\left(\alpha - \tan^{-1}(y/x)\right)\cos\left(\alpha - \tan^{-1}(y'/x')\right) \\
\xi_s^{css}(l,l') &= \cos\left[s\left(\tan^{-1}(y/x) - \tan^{-1}(y'/x')\right)\right] \\
&\quad \cdot \sin\left(\alpha - \tan^{-1}(y/x)\right)\sin\left(\alpha - \tan^{-1}(y'/x')\right), \qquad \text{(C2)}
\end{aligned}$$

with

$$\rho = \sqrt{x^2 + y^2}, \qquad \rho' = \sqrt{x'^2 + y'^2}$$
$$x = x_s + l\cos(\alpha), \qquad y = y_s + l\sin(\alpha) \tag{C3}$$
$$x' = x_s + l'\cos(\alpha), \quad y' = y_s + l'\sin(\alpha).$$

[54] **Acknowledgments.** This work was partially supported by the National Science Foundation under grant ECS-0220218 and NASA EPSCoR Cooperative Agreement NCC5-574. The authors thank the reviewers for their valuable comments.

References

Aas, J. A. (1991), Plane-wave reflection properties of two artificially hard surfaces, *IEEE Trans. Antennas Propag.*, *39*(5), 651–656.

Chew, W. C. (1989), Some observations on the spatial and eigenfunction representations of dyadic Green's functions, *IEEE Trans. Antennas Propag.*, *37*(10), 1322–1327.

Collin, R. E. (1991), *Field Theory of Guided Waves*, IEEE Press, Piscataway, N. J.

Cucini, A., M. Caiazzo, P. Bennati, and S. Maci (2004), Quasi-TEM waveguide by using FSS-based hard surfaces, paper presented at URSI EM Theory Symposium, Union Radio Sci. Int., Pisa, Italy, 23–27 May.

Eshrah, I. A., A. B. Yakovlev, A. A. Kishk, A. W. Glisson, and G. W. Hanson (2004), The TE_{00} waveguide mode: The "complete" story, *IEEE Antennas Propag. Mag.*, *46*(5), 33–41.

Johnson, W. A., A. Q. Howard, and D. G. Dudley (1979), On the irrotational component of the electric Green's dyadic, *Radio Sci.*, *14*(6), 961–967.

Kildal, P.-S. (1988a), Definition of artificially soft and hard surfaces for electromagnetic waves, *Electron. Lett.*, *24*(3), 168–170.

Kildal, P.-S. (1988b), Technical memorandum: Bandwidth of a square hard horn, *IEE Proc. Part H Microwaves Opt. Antennas*, *135*(4), 275–278.

Kildal, P.-S. (1990), Artificially soft and hard surfaces in electromagnetics, *IEEE Trans. Antennas Propag.*, *38*(10), 1537–1544.

Kishk, A. A. (2003), Analysis of hard surfaces of cylindrical structures of arbitrarily shaped cross section using asymptotic boundary conditions, *IEEE Trans. Antennas Propag.*, *51*(6), 1150–1156.

Kishk, A. A., and P.-S. Kildal (1997), Asymptotic boundary conditions for strip-loaded scatterers applied to circular dielectric cylinders under oblique incidence, *IEEE Trans. Antennas Propag.*, *45*(1), 51–56.

Kishk, A. A., and M. Morgan (2001), Analysis of circular waveguides with soft and hard surfaces realized by strip-loaded walls using asymptotic boundary conditions, *Microwave Opt. Technol. Lett.*, *29*(6), 433–436.

Kishk, A. A., P.-S. Kildal, A. Monorchio, and G. Manara (1998), Asymptotic boundary condition for corrugated surfaces, and its application to scattering from circular cylinders with dielectric filled corrugations, *IEE Proc. Part H Microwaves Opt. Antennas*, *145*(1), 116–122.

Lier, E., and P.-S. Kildal (1988), Soft and hard horn antennas, *IEEE Trans. Antennas Propag.*, *36*(8), 1152–1157.

Lindell, I. V. (1995), Image theory for the soft and hard surface, *IEEE Trans. Antennas Propag.*, *43*(1), 117–119.

Maci, S., M. Caiazzo, A. Cucini, and M. Casaletti (2005), A pole-zero matching method for EBG surfaces composed of a dipole FSS printed on a grounded dielectric slab, *IEEE Trans. Antennas Propag.*, *53*(1), 70–81.

Manara, G., P. Nepa, and G. Pelosi (2000), High-frequency EM scattering by edges in artificially hard and soft surfaces illuminated at oblique incidence, *IEEE Trans. Antennas Propag.*, *48*(5), 790–800.

Nepa, P., G. Manara, and A. Armogiba (2001), Electromagnetic scattering by anisotropic impedance half and full planes illuminated at oblique incidence, *IEEE Trans. Antennas Propag.*, *49*(1), 106–108.

QWED (1998), QuickWave3D: A general purpose electromagnetic simulator based on conformal finite-difference time-domain method, version 2.2, Warsaw.

Ruvio, G., P.-S. Kildal, and S. Maci (2003), Modal propagation in ideal soft and hard surface, *IEEE Antennas Propag. Soc. Int. Symp. Dig.*, *4*, 438–441.

Sipus, Z., P.-S. Kildal, and J. Salmonsson (1996), Two-dimentional analysis of bandwidth of open hard surface, *IEE Proc. Part H Microwaves Opt. Antennas*, *143*(6), 475–481.

Skobelev, S. P., and P.-S. Kildal (1998), Blindness removal in arrays of rectangular waveguides using dielectrically loaded hard walls, *IEEE Trans. Antennas Propag.*, *46*(4), 546–550.

Skobelev, S. P., and P.-S. Kildal (2000), Performance of an array of circular waveguides with strip-loaded dielectric hard walls, *IEEE Trans. Antennas Propag.*, *48*(7), 1106–1114.

Viola, M. S., and D. P. Nyquist (1988), An observation on the Sommerfeld-integral representation of the electric dyadic Green's function for layered media, *IEEE Trans. Antennas Propag.*, *36*(8), 1289–1292.

Wang, J. J. H. (1982), A unified and consistent view on the singularities of the electric dyadic Green's function in the source region, *IEEE Trans. Antennas Propag.*, *30*(3), 463–468.

Yaghjian, A. D. (1980), Electric dyadic Green's functions in the source region, *Proc. IEEE*, *68*(2), 248–263.

Yaghjian, A. D. (1982), A delta-distribution derivation of the electric field in the source region, *Electromagnetics*, *2*, 161–167.

Yang, F.-R., K.-P. Ma, Y. Qian, and T. Itoh (1999), A novel TEM waveguide using uniplanar compact photonic-bandgap (UC-PBG) structure, *IEEE Trans. Microwave Theory Tech.*, *47*(11), 2092–2098.

I. A. Eshrah, A. W. Glisson, A. A. Kishk, V. A. Klymko, and A. B. Yakovlev, Center for Applied Electromagnetic Systems Research, Department of Electrical Engineering, University of Mississippi, University, MS 38677-1848, USA. (ieshrah@olemiss.edu; aglisson@olemiss.edu; ahmed@olemiss.edu; vick@olemiss.edu; yakovlev@olemiss.edu)

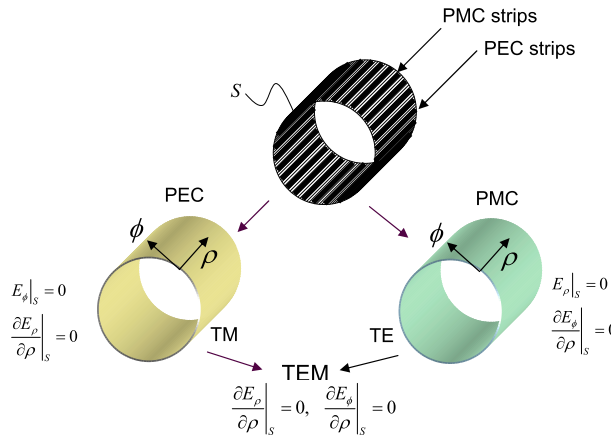

Figure 1. PEC/PMC strip model for an ideal hard surface circular waveguide. The hard surface behaves like a PEC waveguide for TM modes and as a PMC waveguide for TE modes. A TEM mode is obtained as a contribution of TM and TE modes in the zero-cutoff limit. The TEM mode "sees" the ideal hard surface waveguide as a combination of PEC and PMC waveguides, and it satisfies the boundary conditions on the ideal hard surface partially contributed by PEC and PMC waveguides, that is, $\partial E_\rho/\partial \rho|_S = 0$, $\partial E_\phi/\partial \rho|_S = 0$.